# Influence of Al and F Surface Modifications on the Sudden Death Effect of Si-Gr/Li1.2Ni0.2Mn0.6O2 Li-Ion Cells

David Peralta, Jérémie Salomon, Jean-Frederic Martin, Eric de Vito, Jean-François Colin, Adrien Boulineau, Carole Bourbon, Benjamin Amestoy, Celine Tisseraud, Roger Pellenc, et al.

# Influence of Al and F Surface Modifications on the Sudden Death Effect of Si-Gr/$Li_{1.2}Ni_{0.2}Mn_{0.6}O_2$ Li-Ion Cells

David Peralta,*,† Jérémie Salomon,† Yvan Reynier,† Jean-Frédéric Martin,† Eric De Vito,† Jean-François Colin,† Adrien Boulineau,† Carole Bourbon,† Benjamin Amestoy,† Celine Tisseraud,† Roger Pellenc,‡ Jean-Louis Ferrandis,‡ Didier Bloch,† Sébastien Patoux†

† Univ. Grenoble Alpes, F-38402 Saint Martin d'Hères, France. CEA, LITEN, F-38054 Grenoble, France.

‡ PELLENC ENERGY SAS, Quartier Notre Dame, Route de Cavaillon, 84120 Pertuis

Corresponding author: david.peralta@cea.fr

## Graphical Abstract

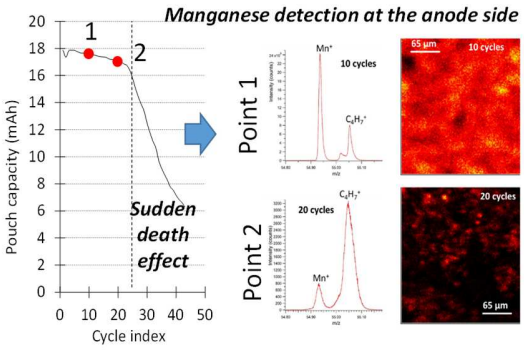


## Highlights

- Dissolution, migration and deposition (DMD process) is observed in silicon-graphite/lithium rich Si-Gr/$Li_{1.2}Ni_{0.2}Mn_{0.6}O_2$ systems
- $AlF_3$ coating do not avoid the manganese dissolution process
- Al and F elements dope the lithium layered surface structure

## Keywords

Cathode; Lithium batteries; Coating; Lithium-rich materials

## Abstract

The dissolution, migration and deposition (DMD process) of transition metal ions during cycling is a well-known phenomenon reported in literature especially concerning high manganese spinel cathode material. The main approach to solve this issue consists in coating or doping the particles surface with electrochemically inert cations and/or anions. In this study, we describe a DMD process mechanism which happens in the silicon-graphite/lithium rich layered oxide (Si-Gr/$Li_{1.2}Ni_{0.2}Mn_{0.6}O_2$) systems. This phenomenon leads to a sudden death effect of the cell after 25 cycles. $AlF_3$ coating is envisaged to limit the cation dissolution from the positive electrode: we highlight that our synthesis finally results in improving the electrochemical performances of lithium rich layered oxides by offering an Al/F doped surface. Despite this improvement, the coating fails, on the other hand, to stop the transition metal cations dissolution, especially in Li-ion cells (Si-Gr as anode).

## 1. Introduction

The expected expansion of Electrified Vehicles (EV) in the coming years gives rise to the question of how to produce low-cost and environmentally friendly batteries. In 2020, global passenger car sales reached 1.9 M units BEV and 0.5 M units PHEV. It is forecasted that by 2030, BEV will increase to 7.3 M units and 0.8 M units PHEV [1]. Even if this new transport technology is a real opportunity to improve air quality in cities, the limitation of the dependence on critical and toxic materials such as cobalt is one of the key success to consider this technology as a green solution. Moreover, a significant increase of the acceptance of EVs can only come via both an increase of the driving range and a significant cost reduction. These two last specifications are at the origin of the current “high energy density race” and of the development of new high-energy cathode materials. Currently, the most promising materials that can cope with all these specifications belong to the lithium-rich layered oxides family.

Lithium-rich layered oxides are cobalt-free materials, and offer high specific energies and capacities (>250 mAh/g). The structure of these materials is a matter of debate in the scientific community. When some researchers describe the lithium-rich layered structure as a solid solution, others lean towards a composite structure built of $LiMO_2$ and $Li_2MO_3$ domains (M = Mn, Ni) [2-7]. Complex electrochemical

reactions result from this special structure. As an example, in the well-known $Li_{1.2}Ni_{0.2}Mn_{0.6}O_2$ composition, the manganese is at the 4+ oxidation state; so that only $Ni^{2+}$ could be oxidized at such level during electrochemical oxidation. Thus, considering the $Ni^{2+}/Ni^{4+}$ redox couple, only 0.4 lithium can be removed from the structure, and this can only explain 126 mAh/g of the total specific capacity. Many researchers worked to understand the reason of the extracapacity. Some authors demonstrated that a part of the oxygen of the structure can evolve in peroxo/superoxo-like species and can cycle reversibly [8-12]. Despite its numerous advantages, the lithium-rich layered oxides suffer from a structure evolution when the cell is cycled above 4.3V [13-17]. This phenomenon induces a progressive fade of the cell working voltage and a loss in energy density during cycling. Other drawbacks such as low C-rate capability and high first irreversible capacity could also be pointed out. Some studies highlight that surface treatments can enhance electrochemical performances of lithium-rich layered oxides. Metal oxide, phosphate and fluoride coatings are mainly used in the literature [18-37]. Among all these surface treatments, $AlF_3$ appears as a very promising post treatment for lithium-rich layered oxide. Several publications report that $AlF_3$ coatings can increase both the capacity and the C-rate capability of the cathode material [31-34]. Moreover, some authors claim that $AlF_3$ treatment can alleviate the voltage fade issue of the cathode material [37]. However, a large part of the literature conclusions are based on Li-metal half-cells experimental results, and some significant discrepancies could be observed between half and full cells.

The purpose of this paper is to investigate the influence of $AlF_3$ surface treatments in half-cells but also in Li-ion cells. It is observed that the capacity suddenly decays after 20 cycles due to manganese dissolution. A main part of this paper is dedicated to discussing the influence of the DMD process.

## 2. Experimental

### 2.1. Synthesis

All materials were synthesized by using commercial reactants: nickel sulfate hexahydrate (Sigma Aldrich®,$NiSO_4.6H_2O$, 99%), manganese sulfate monohydrate (Sigma Aldrich®, $MnSO_4$ $H_2O$, 99%), lithium carbonate (Sigma Aldrich®, $Li_2CO_3$, 99%) and sodium carbonate (Sigma Aldrich®, $Na_2CO_3$,

99.95%), aluminium nitrate nonahydrate (Acros Organic®, $Al(NO_3)_3.9H_2O$) and ammonium fluoride (Prolabo®, $NH_4F$, 98%). All reactants were used without further purification.

*Synthesis of $Li_{1.2}Ni_{0.2}Mn_{0.6}O_2$.* In order to compare the coating influence with the best possible accuracy, the same batch of pristine material is used (1 kg batch). The synthesis protocol of $Li_{1.2}Ni_{0.2}Mn_{0.6}O_2$ is adapted from Peralta et al. to produce 1 kg of oxide [15]. 6.25 mol of $NiSO_4.6H_2O$ and 18.75 mol of $MnSO_4.H_2O$ are mixed in 25 L of water. In another container, 25 mol of $Na_2CO_3$ and 5 mol of $NH_4OH$ are mixed in 25 L of deionized water. The transition metal ion solution is pumped directly into a 65 L CSTR reactor and the pH is kept at 7.5 during the whole synthesis by injecting the carbonate solution. Then, the final solution of the CSTR is aged for 7 h. Afterward, the carbonate of nickel and manganese ($Ni_{0.25}Mn_{0.75}CO_3$) is recovered by filtration. The product is washed several times with hot water in order to remove residual sodium and sulfate species and finally, the carbonate is dried in an oven at 120 °C during one night. To obtain the final $Li_{1.2}Ni_{0.2}Mn_{0.6}O_2$ material, $Ni_{0.25}Mn_{0.75}CO_3$ is intimately mixed with an excess (3.3%) of lithium carbonate ($Li_2CO_3$) and the mixture is fired at 900 °C during 24 h.

*$AlF_3$ treatment.* In the text, the coating ratio represents the molar ratio between the metal fluoride and the pristine materials. The same synthesis protocol is used to produce the different coating ratio. As an example, to produce 1% $AlF_3$-treated $Li_{1.2}Ni_{0.2}Mn_{0.6}O_2$, 2.73 g of $Al(NO_3)_3.9H_2O$ are dissolved in 1L of water. Then 60 g of $Li_{1.2}Ni_{0.2}Mn_{0.6}O_2$ are dispersed in this solution and the resulting mixture is heated at 80 °C. Then a solution of 0.81 g of $NH_4F$ dissolved in 400 mL of water is added drop by drop in the first solution. The temperature is maintained during 5 hours then the product is recovered by filtration. The resulting powder is treated at 400 °C for 5 h.

### 2.2. Characterisation

*XRD.* Crystallinity of materials is controlled by X ray diffraction technique (XRD) using a Brüker AXS D8 diffractometer equipped with a Cu anticathode ($K\alpha_{1,2}$).

*Microscopy.* Materials are observed by Scanning Electron Microscopy (SEM) by dispersing the powders on carbon tape using a LEO 1530 SEM. EDX mappings are performed using a FEI Tecnaï OSIRIS operating at 200 kV in STEM mode and equipped with SuperX EDX detector system.

*Surface analysis.* After cycling, electrodes are retrieved from the cell and washed inside a glovebox with Dimethyl Carbonate. Their transfer is achieved by using an airtight vessel to a PHI VersaProbe II (Physical Electronics instrument) or a TOF.SIMS5 spectrometer (Ion Tof instrument). Charging effects are controlled during XPS analysis with a combination of low energy electron gun (negative charge) and low energy argon gun (positive charge). The X-ray source is an Al Kα monochromatic beam (1486.7 eV), the takeoff angle is set at 45°. High resolution spectra are acquired at an energy resolution of ~0.6 eV. All spectra are calibrated by using F 1s as a reference binding energy for F in LiF (685 eV). TOF-SIMS characterisation are also achieved by using a load-lock compatible with the same air-tight transfer vessel as described above. Analyses were carried out in a positive polarity mode to achieve the elemental mappings of Mn and Ni at the electrodes surface. The primary ion beam is $Bi^+$ set at 30 kV.

*Electrochemical characterisations.* The first electrochemical tests are carried out using standard CR2032 type coin cells assembled in an argon-filled glove box. Electrodes are prepared by mixing $Li_{1.2}Ni_{0.2}Mn_{0.6}O_2$ (80 wt%), C65 (10 wt%) as conductive additive, and PVDF (10 wt%) as binder agent. After grinding in hexane, the powder is dispersed in N-methyl-2-pyrrolidone, coated on an aluminium foil and then dried at 80 °C under vacuum for 48 h. Disks of 14 mm diameter are punched from the foil, and pressed at 650 MPa. The electrode is then used as positive electrode in a coin cell comprising lithium foil as the negative electrode, one Celgard 2400 and one Viledon® as separators soaked in electrolyte. Specific capacities and current rates are calculated based on a specific capacity of 316 mAh per gram of $Li_{1.2}Ni_{0.2}Mn_{0.6}O_2$.

10 $cm^2$ pouch cells are manufactured to evaluate cycle life in full cell configuration: they are assembled in a -20°C dew point dry room with one single layer positive electrode (3.2 x 3.2 cm active area), a separator (Celgard 2320 of 20 µm of thickness) and an oversized negative electrode (3.5 x 3.5 cm). The positive electrode is made with 92 %wt active material, 4% conductive additive and 4%

PVDF, coated on 20 µm Al foil using a custom roll to roll equipment and NMP solvent. The negative electrode coated on 10 µm copper foil has 94%wt active material (95 wt% of graphite and 5 wt% of silicon nanoparticle), 2% conductive additive, 2% CMC and 2% SBR binder and is based on an aqueous formulation. After drying under vacuum at 55°C overnight, they are transferred in an argon atmosphere glove box for electrolyte filling with $LiPF_6$ 1M in EC/DMC/EMC (1/1/1 vol.) + 10% FEC (EC: Dimethyl carbonate, EC: Ethylene carbonate, EMC: Ethyl methyl carbonate, FEC: Fluoroethylene carbonate). The cathode loading is fixed at 10 mg/cm² and the anode loading is adjusted to 6 mg/cm² resulting in a maximum N/P of 1.05.

*Gas Chromatography Mass Spectrometry (GCMS).* For electrolyte analysis, the GCMS (Agilent 7890 with column DB-200 122-2032 30 m x 0.25 mm 0.25 µ) is used with a split 100 injection mode at 280°C. The column ramp is 40°C to 200°C at 10°C/minute. The electrolytes are sampled in the pouch cells and diluted in acetonitrile. DMC and EMC are too volatile and their measured quantities are too dependent on the cell opening conditions for reliable results. For this reason, we only consider the FEC/EC ratio because the cyclic carbonates measures (integrated surface of total ion count peak calibrated with pure solvents) are less sensitive and permit to follow FEC consumption.

## 3. Results

### *3.1. Characterisation of lithium-rich pristine material*

A 1kg-batch of $Li_{1.2}Ni_{0.2}Mn_{0.6}O_2$ is prepared by a coprecipitation method on a pilot reactor. The material is characterized by XRD and resulting unit cell parameters are very close to those observed in literature (see Figure 1a) [15]. The compound crystallizes in the *C2/m* space group and no extra peak corresponding to any impurity phases is observed. All peaks, except for those between 20 and 25° correspond to a layered oxide structure based on a hexagonal α-$NaFeO_2$ structure (space group $R\bar{3}m$). The peaks between 20 and 25° result from the ordering of the lithium ions with the M ones in the transition-metal layers, and provide the structure with $Li_2MnO_3$-type features (space group *C2/m*). As expected for a synthesis based on a co-precipitation method, a SEM picture (Figure 1b) reveals that dense, spherical particles are obtained. Primary particles of ~200 nm are aggregated in dense secondary

particles of ~ 6 µm diameter. The electrochemical performances of the as made $Li_{1.2}Ni_{0.2}Mn_{0.6}O_2$ are evaluated in half-cells in galvanostatic mode using 0.1 C rate between 4.8 V and 2.5 V. The first charge/discharge curve in Figure 1c has a classical shape and reveals performances at the state of the art (272 mAh/g in charge and 204 mAh/g in discharge – 25 % of irreversibility). The capacity slowly increases up to 240 mAh/g during the first cycles and the voltage decay has two different slopes (Figure 1d). This phenomenon is already documented in literature and could be attributed to the activation of $Li_2MnO_3$ domains of the composite structure [15,38].

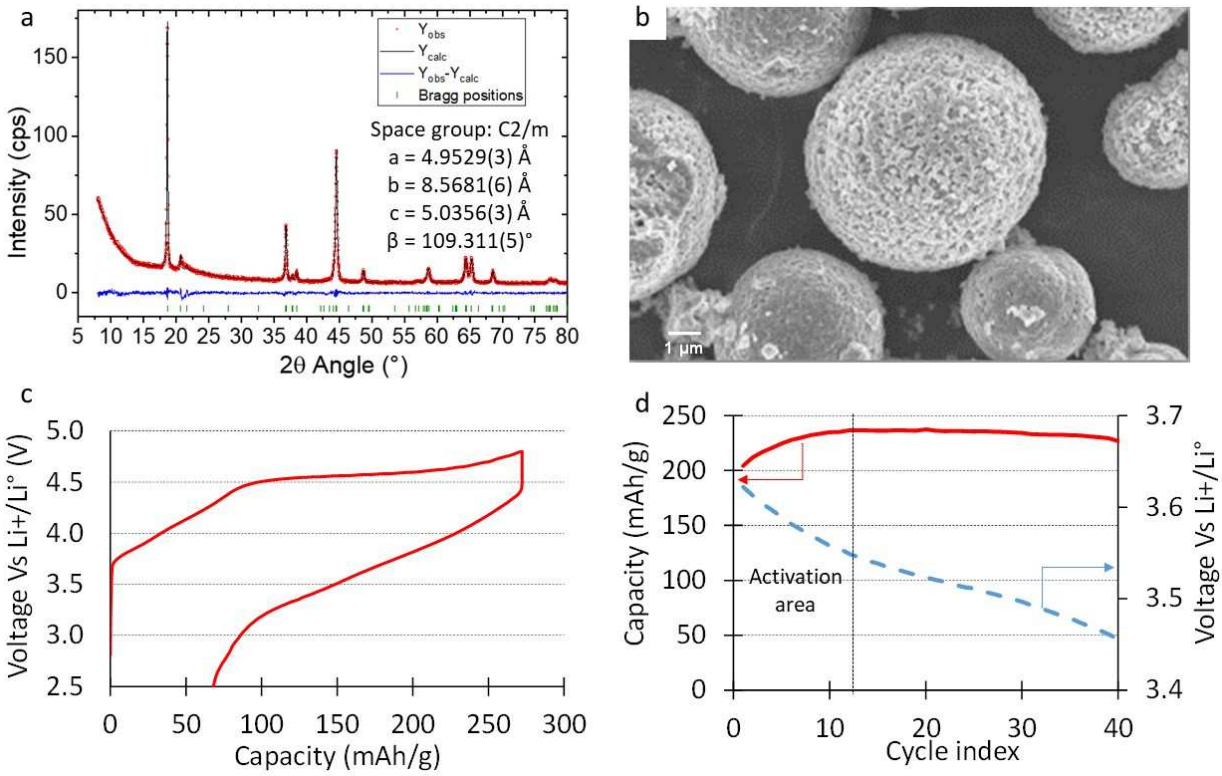


Figure 1. $Li_{1.2}Ni_{0.2}Mn_{0.6}O_2$ physicochemical characterisations: (a) XRD pattern, (b) SEM image, (c) First charge and discharge curves (d) Discharge capacities and discharge average voltage versus cycle number of lithium-rich coin cells

The electrochemical performances of the material are investigated in Li ion pouch cells using a silicon-graphite anode. Because of the slow activation process observed in half coin cells, it was decided to submit pouch cells to several conditioning methods at C/10. The first conditioning method consists in

making 3 cycles between 4.7 V and 2.5 V (Vs Si-Gr). The second and the third methods consist in charging and maintaining the pouch cell at a constant voltage of 4.5 V (CC/CV until C/50) at room temperature (method 2) and at 45 °C (method 3). After the formation step, all cells are cycled between 4.4V and 2.5V at C/3 (Figure 2a&b). Best results are obtained with the cell formed with 3 cycles at 4.7 V (18 mAh Vs 16 and 14.7 mAh respectively for method 2 and 3). After 25 cycles, both capacities and average voltages of all cells suddenly fade. This surprising phenomenon will be called "sudden death effect" in this paper. The Figure 2c represents the difference between the average voltage in charge and discharge and provide some indications about the cells polarization. Curiously, the resistance of the cells suddenly increases after 25 cycles.

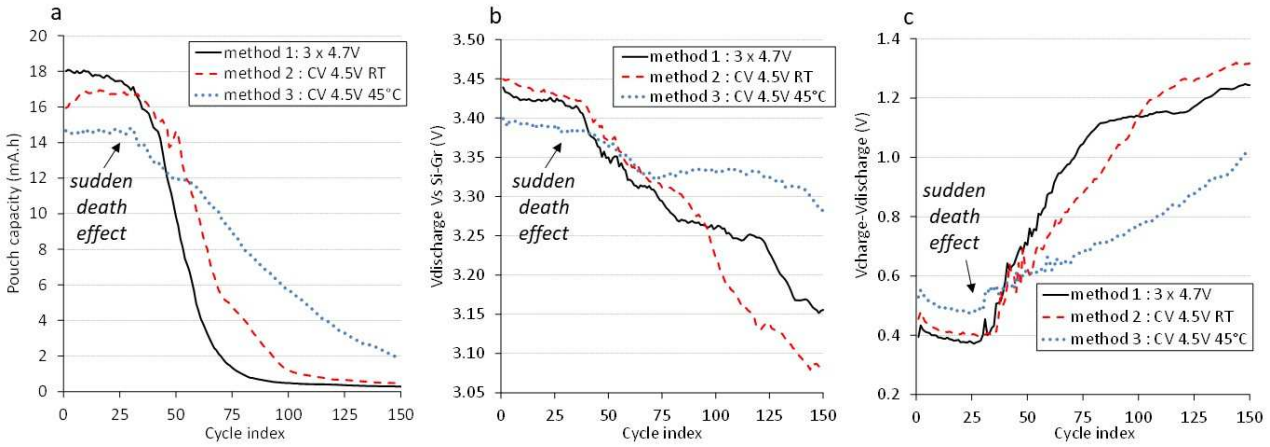


Figure 2. Influence of different activation methods on Si-Gr/$Li_{1.2}Ni_{0.2}Mn_{0.6}O_2$ pouch cells cycle life: (a) Capacity, (b) Average voltage in discharge, (c) difference between the average voltage in charge and discharge as a function of cycle number

The first hypothesis in front of such a results was to incriminate the electrolyte stability. GCMS and gas release measurements were performed on the electrolyte just after the formation step and after cycling. GCMS results are summarized in the Table 1.

Table 1. GCMS results and gas released by electrolyte of pouch cells as a function of the activation process

| | End of formation | End of cycling |
|---|---|---|

| | FEC/EC | Gas release | FEC/EC | Gas release |
|---|---|---|---|---|
| Method 1 | 0.23 | 0.6 | 0.22 | 0.5 |
| Method 2 | 0.26 | 0.7 | 0.21 | 0.7 |
| Method 3 | 0.23 | 1.8 | 0.17 | 2.0 |

There is a visible consumption of FEC (FEC/EC initial value is 0.3) during formation. This consumption is higher when the formation step includes high voltages or high temperature. However, high voltage does not promote gas formation while the 45°C method produces 3 times more gas than the room temperature methods. The FEC/EC ratio is evolving after 150 cycles but we cannot make reliable conclusions, as the capacity retention is not the same for the three conditioning methods. Room temperature condition for cycling does not promotes gas formation and values are the same as after formation. Looking at the chromatograms, no additional degradation product is detected in the electrolyte. Based on these observations we can support the assumption that the electrolyte decomposition is not the cause of the sudden death effect. It seems more credible to incriminate active materials of the cells. Because some Si-Gr anodes exhibit poor cycle lives, we test our anode in front of a commercial grade of NMC 622. No sudden death effect is observed and we can conclude that the Si-Gr material used in this study is not the cause of the quick capacity fade (Figure S1 in supplementary information file). Literature reports that elements from high manganese content materials can be dissolved in the electrolyte during cycling and these elements can migrate and poison the anode [39].

### *3.2. Characterisation of lithium-rich material after $AlF_3$ treatment*

The manganese dissolution is well documented in the literature concerning spinel materials. It is generally demonstrated that the dissolution is due to a surface mechanism. We decided to treat our material with $AlF_3$ coatings in order to solve the sudden death effect. 60 g of $Li_{1.2}Ni_{0.2}Mn_{0.6}O_2$ is coated with different amounts of $AlF_3$. No additional peak can be observed in XRD. The amount of $AlF_3$ is certainly too low to be observed by XRD (Figure 3a), but the electrochemical behavior is clearly modified. An optimum is obtained with an $AlF_3$ treatment of 1%: 280 mAh/g are obtained for the first discharge in comparison of 205 mAh/g obtained for the pristine material and the irreversible capacity

decreases from 25 % to 11% (Figure 3 b&c). It can also be noticed that the $AlF_3$ treatment does not solve the voltage decay issue (Figure 3d).

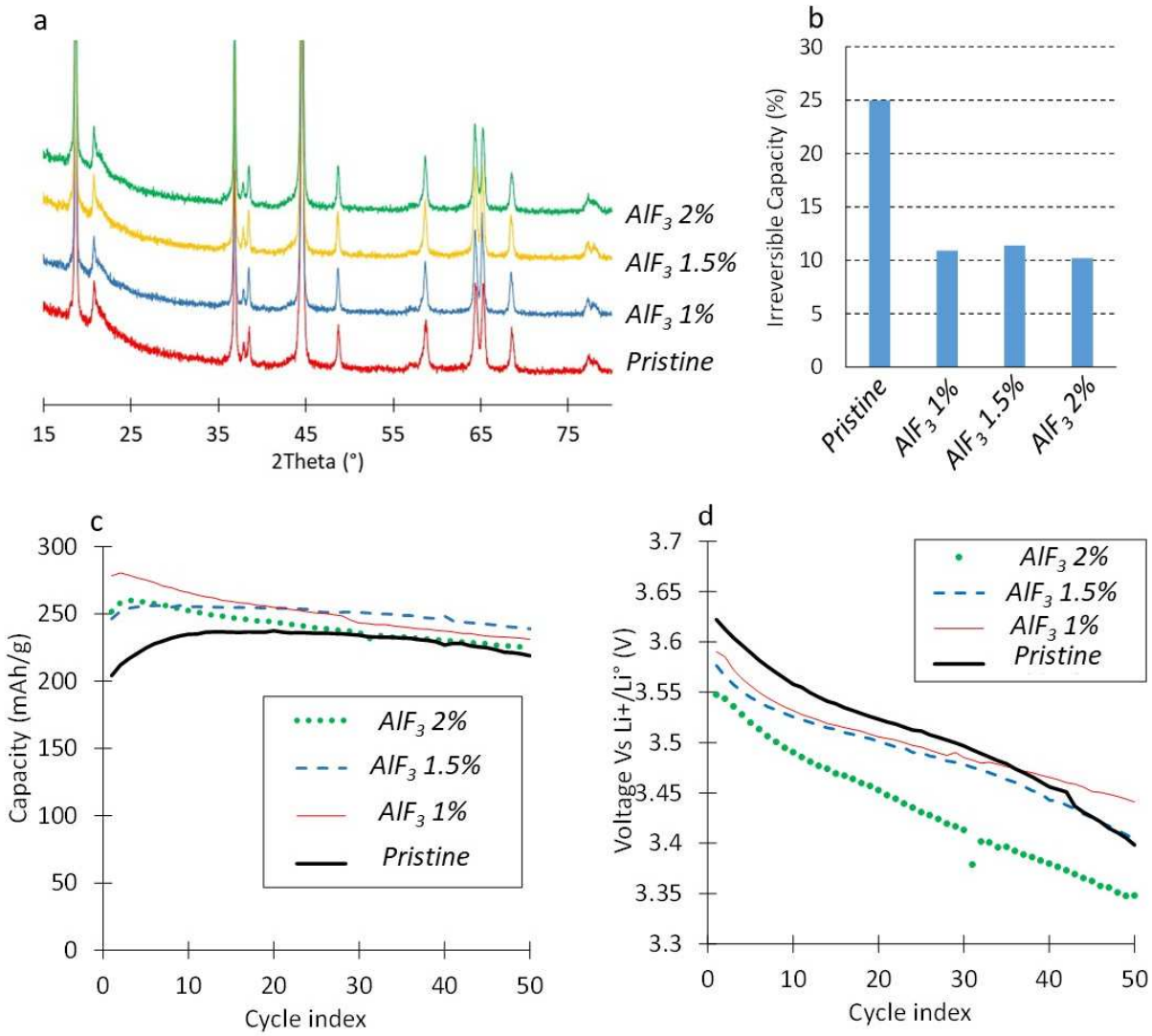


Figure 3. Characterisation of $AlF_3$-treated $Li_{1.2}Ni_{0.2}Mn_{0.6}O_2$: (a) XRD patterns, (b) influence of the $AlF_3$ amount on the first irreversible capacity, (c & d) Discharge capacities and discharge average voltage versus cycle number of coin cells

STEM-EDX is performed on all samples in order to confirm the presence of aluminum and fluor in particles. The mappings achieved confirm the good homogeneity of aluminum and fluor on particles and we can conclude that we successfully modified the pristine material surface (Figure 4).

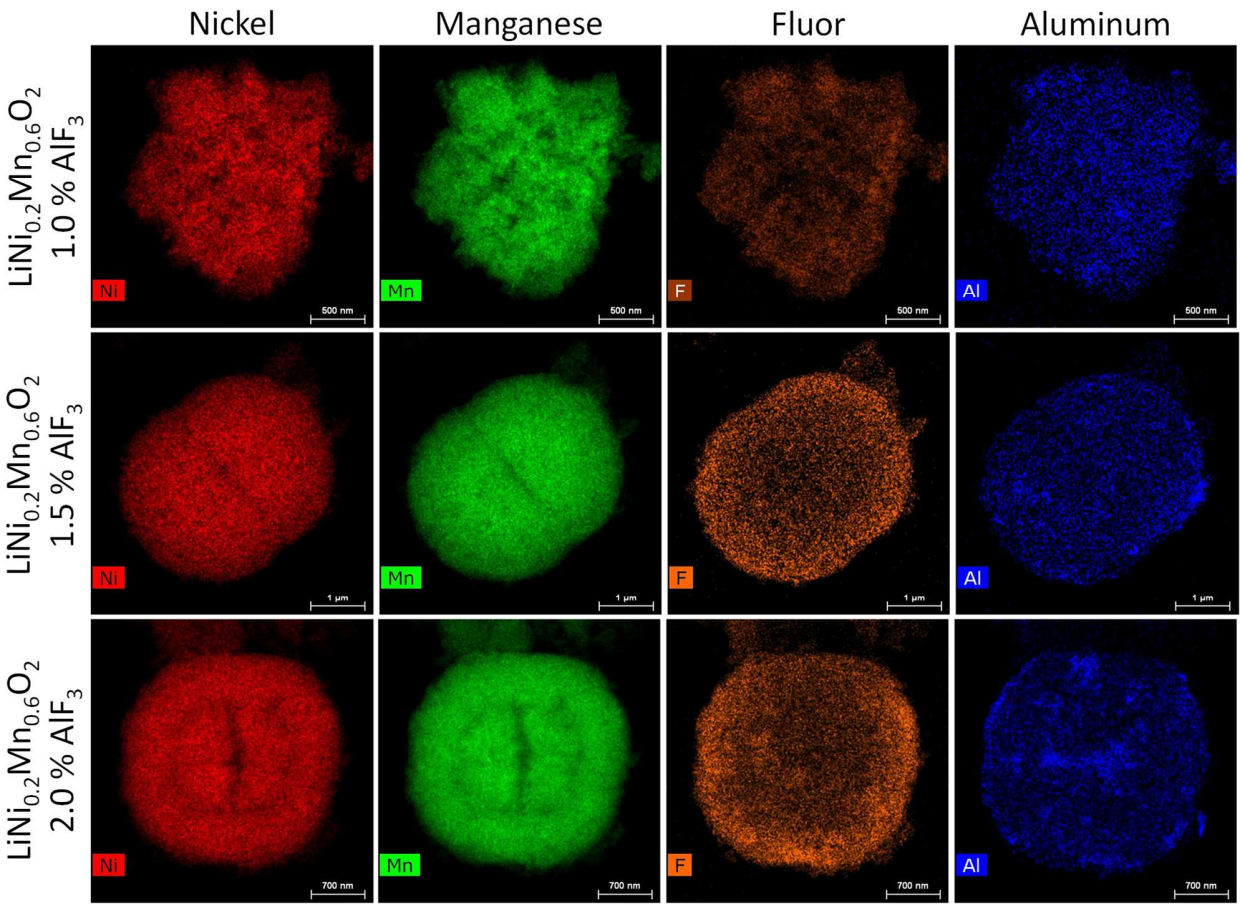


Figure 4. Chemical mappings obtained from STEM EDX experiments with the $AlF_3$-treated materials

Pouch cells are produced and tested in galvanostatic mode following the method 2 of conditioning. The higher capacity is obtained with 1% of $AlF_3$ which is in good agreement with the results obtained in coin cells (Figure 5a).

Capacities of all materials remain stable only during 25 cycles and then, decay quickly due to an increase of the cell polarization (Figure 5c). Similarly to our previous observation in coin cells, we can conclude that our $AlF_3$ coatings do not solve the voltage decay issue (Figure 5b). Unfortunately, the sudden death effect is not suppressed by the surface treatment.

Pouch cells were cycled and anodes were characterized by XPS after 10 cycles and 20 cycles (just before the sudden death effect).

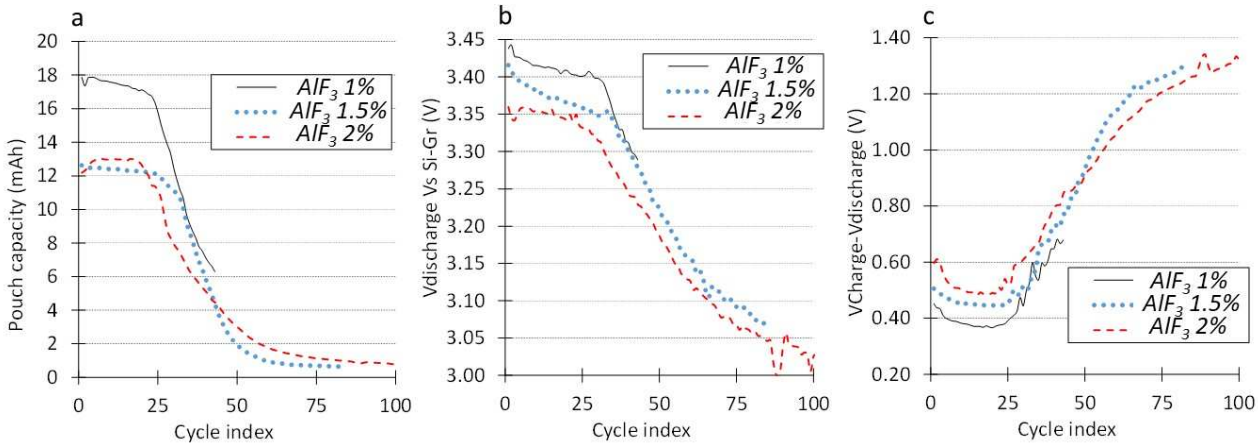


Figure 5. Influence of $AlF_3$ treatments on Si-Gr/$Li_{1.2}Ni_{0.2}Mn_{0.6}O_2$ pouch cells cycle life: (a) Capacity, (b) Average voltage in discharge, (c) difference between the average voltage in charge and discharge as a function of cycle number

XPS results of cycled negative electrodes in front of $AlF_3$-coated cathodes are reported on Figure 6. First, it is important to note that Al is never observed at the anode side. From Table 2 it is noticed that the SEI is mainly composed of C, O and Li, F concentration remaining below 3%.

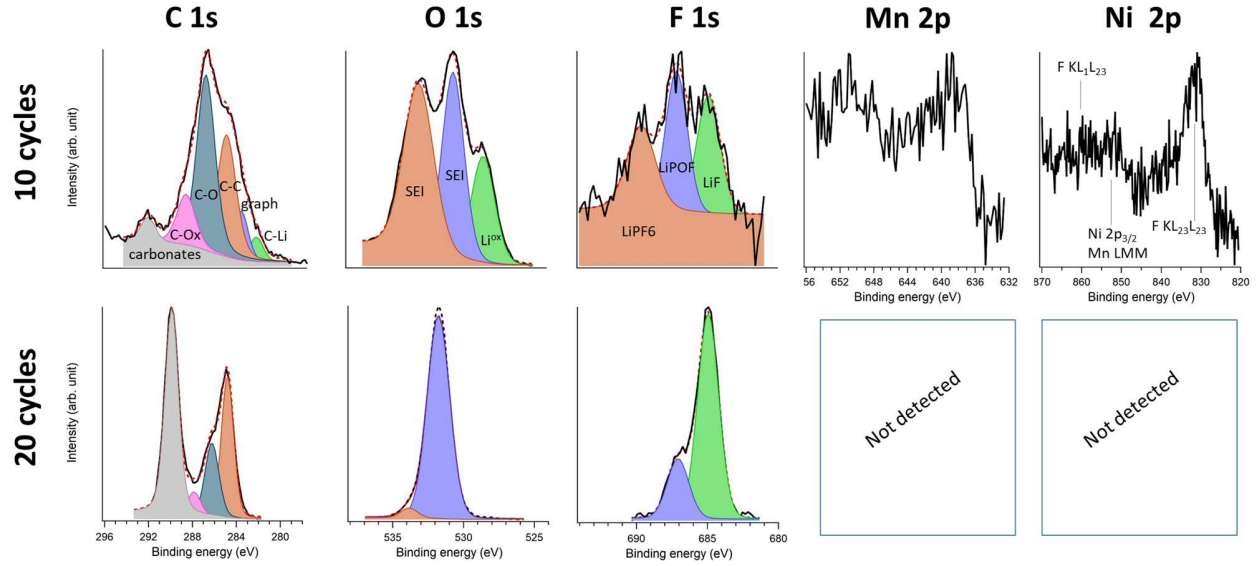


Figure 6. XPS spectra of negative electrodes (Si-Gr/$Li_{1.2}Ni_{0.2}Mn_{0.6}O_2$ pouch cells) after electrochemical cycling (10 and 20 cycles)

Table 2. Composition of the XPS probed volume (atomic%) as a function of cycling

| Cycle index | Li | C | O | F | P | Mn | Ni |
|---|---|---|---|---|---|---|---|
| 10 | 44.7 | 26.6 | 26.5 | 1.6 | 0.3 | 0.3 | Traces |
| 20 | 26.7 | 25.6 | 44.3 | 2.9 | 0.5 | - | - |

However the balance between those elements is quite different after 20 cycles (compared to the situation after 10 cycles). After 10 cycles, C 1s spectrum exhibits several peaks. The low-binding energy peak observed after 10 cycles points out some trapped Li in graphite [40]. Graphite peak confirms that the SEI at that state is still thin (graphite photoelectrons are not screened). The peaks located between 285-288 eV range are related to organic degradation products like RO-CO2-Li, and the high energy peak to carbonates products [41]. In that case, the balance is clearly in favour of the first category of products. The O 1s spectrum reveals the presence of Li oxides together with oxygen involved in the SEI (again, mainly Li alkyl carbonates species) [42,43]. F 1s peak also exhibits 3 peaks. The low binding energy peak reveals the presence of LiF in low quantities, the other peaks being related to either lithium fluorophosphates degradation products or to traces of $LiPF_6$ not perfectly washed out from the surface of the electrode [44]. Mn and Ni are also detected. In the case of Ni though, the Ni 2p3/2 peak is overlapped with F KLL Auger transition, thus difficult to point out, even if a small peak can be pointed out at ~852 eV (though it could also be a Mn LMM Auger transition, it fits the detection of a Ni+ peak by TOF-SIMS as presented thereafter). The Mn 2p3/2 peak position at ~638 eV indicates that Mn is probably in a metallic form at this stage (Mn(0)) [45].

After 20 cycles: the C-Li peak disappears, while the carbonates peak is more intense. It is noteworthy that the carbonates peak is shifted to higher binding energy, which can be explained by a variation of chemical environment in the SEI. Carbonates can give rise to peaks at up to 292 eV [46,47]. This obviously underlines that the SEI is thicker and has a different composition (involving a higher

carbonates concentration). O 1s peak also shows the disappearance of the Li-O contribution, which is probably related to the increase of the SEI thickness. At the same time, the F 1s spectrum shows a relative increase of the LiF contribution. All these observations point out an evolution of the composition of the SEI during the 10 last cycles. Mn and Ni are also now not detected after 20 electrochemical cycles.

In order to confirm the XPS detection of Mn and Ni, the surface of the cycled electrode is analysed with TOF-SIMS. Results are presented on Figure 7 Even though this is not a quantitative method, its higher sensitivity compared to XPS allows to detect very low amounts of Mn and Ni. After 10 cycles, $Mn^+$ and $Ni^+$ mass peaks are unambiguously detectable; their intensity are respectively at 2.5 104 and 2.103 counts. Such result confirm the presence of Mn and Ni at the surface of the electrode. Moreover, the mapping of both elements shows a relative homogeneity of their surface distribution. After 20 cycles, $Mn^+$ and $Ni^+$ mass peaks are still detectable, though at much lower intensities, falling down to respectively 800 and 100 counts. This explains why Mn and Ni are undetectable by using XPS: their surface concentration fall down below the XPS detection limit for each orbital (Mn 2p and Ni 2p). Surface distribution is also more heterogeneous. These TOF-SIMS results unambiguously confirm the XPS results revealing the presence of Mn and Ni at the surface of the electrodes after 10 cycles, and the absence of detection after 20 cycles.

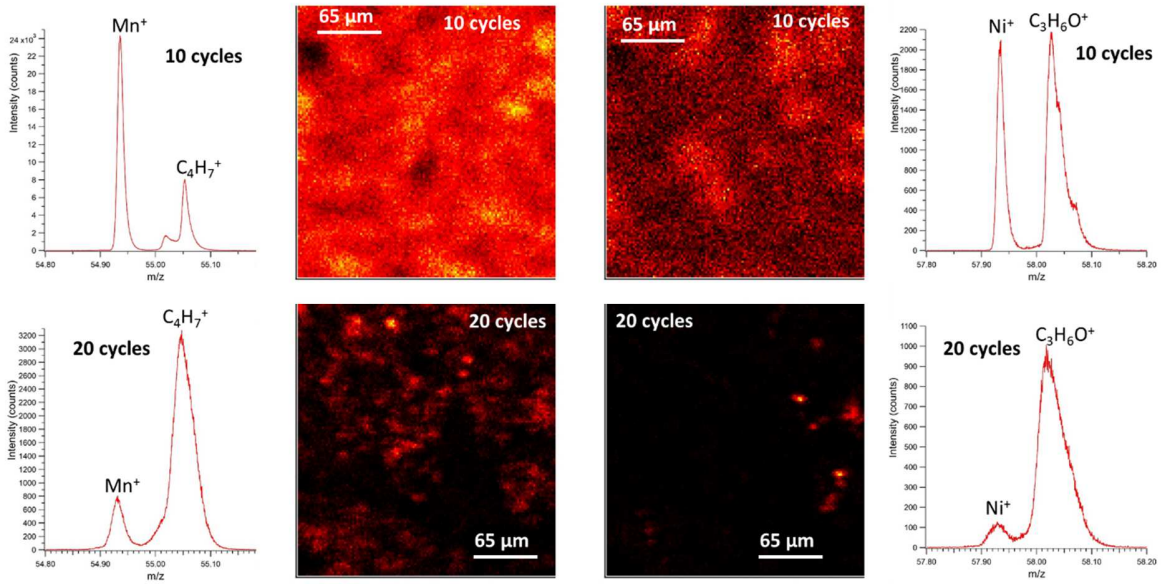


Figure 7. TOF-SIMS mappings of the surface of electrodes for $Mn^+$ (left) and $Ni^+$ (right) after 10 cycles and 20 electrochemical cycles. Mass spectra relative to the maps are presented to the left for $Mn^+$ and to the right for Ni

The first important result to point out is the different SEI chemistries after 10 cycles and 20 cycles. The detection of both manganese and nickel after 10 cycles suggests that these elements are dissolved in the electrolyte and migrate from the cathode side to the anode side. This phenomenon has been already reported in literature by several authors, first for spinel $LiMn_2O_4$ and more recently for 5V spinel material and Li-rich materials [48-51]. Transition metals are known to poison the anode surface [52]. This migration probably happens during the first cycles. Then, the SEI grows on the electrode surface, which makes the detection of Mn and Ni impossible by XPS. The SEI growth is heterogeneous which makes Mn and Ni TOF-SIMS detection also more heterogeneous.

Now the remaining question is how nickel and manganese can be dissolved and migrate through the $AlF_3$ modified surface (Al is never detected at the anode side). STEM-EDX mappings are performed on cathode primary particles to confirm the good homogeneity of fluor and aluminum species (Figure 8a). Then cross sectional analyses are performed along a secondary particle (Figure 8b) and on the surface of the particles (Figure 8c). To fit with a perfect coating, it is expected that first the aluminum and fluor

contents increase and then decrease (due to the pure $AlF_3$ layer) and, only after, the manganese and nickel contents start to increase (due to material bulk). Curiously, no thin peaks of aluminum and fluor can be observed and manganese, nickel, aluminum and fluor start to be detected at the same time. Moreover, classical coatings reported in literature have only several nanometers of thickness. In our case, aluminum and fluor could be detected during 200 nm.

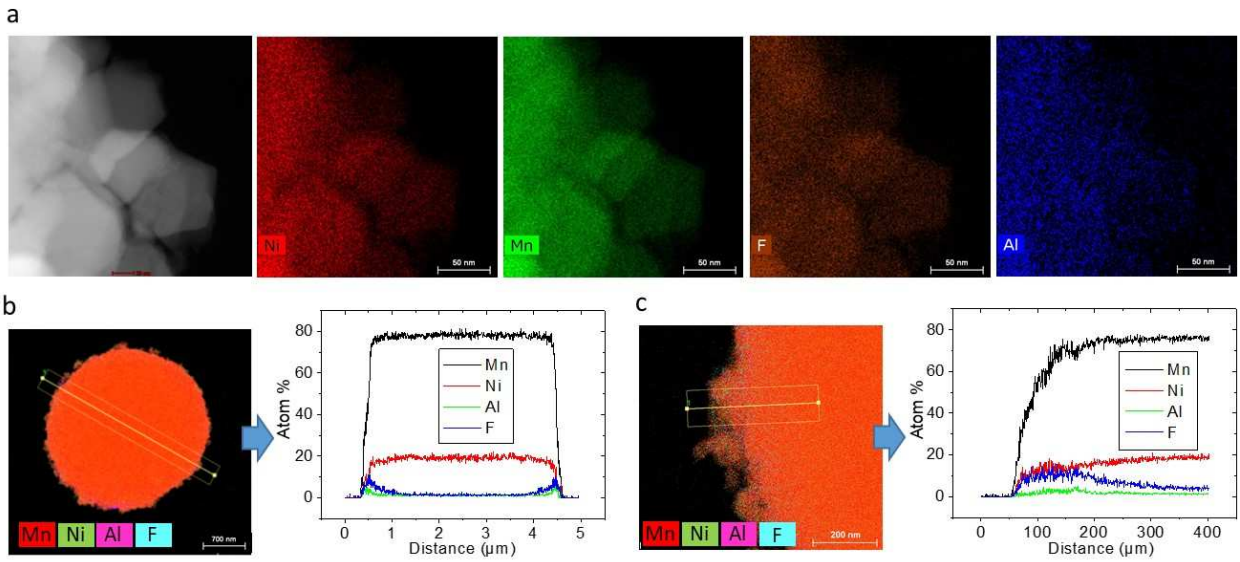


Figure 8. (a) Chemical mappings obtained from STEM EDX experiments performed with the 1% $AlF_3$ treated material before cycling, (b) Profile extracted across a secondary particle, (c) Profile extracted over the surface of a primary particle

It seems that aluminum and fluor do not form an $AlF_3$ layer at the material surface. Aluminum and fluor migrate within the material and dope the structure surface of the external primary particles. TEM images of the lithium-rich layered oxide particles are shown in supplementary information file (Figure S2). It is clear that no additional layer can be observed at the particles surfaces and confirms that aluminum and fluor dope the structure instead of creating a protective layer.

**4. Discussion**

Surface doping/coating: Several publications describe $AlF_3$ surface treatment as an adequate solution to solve the batteries cycle life issue and as a good solution to improve the cell electrochemical performances [31-33,37,53]. Following a similar protocol to what is described in the literature, we

produce here several materials with different $AlF_3$ amounts. Concerning the electrochemical performances, our results are in good agreement with literature. The first irreversible capacity is lower and the specific capacity is higher. However, the cycle life is not improved in Li-ion cells. Using a similar process as ours, several authors observe the formation of a real layer of $AlF_3$, whereas we observe that aluminium and fluor diffuse within the surface structure of the material. Rosina et al. already evoke the possible migration of aluminium inside the Li-rich layered oxide structure and conclude that the $AlF_3$ coating process finally leads to a fluorinated $Al_2O_3$ spinel-like phase [54]. Liu et al. report similar conclusions by observing nanoislands of $Al_2O_3$ with Fluor [55]. We continue to investigate why the results of this synthesis process can lead to such different results as a function of authors. We are now investigating possible side reactions during the heat treatment process, maybe induced by the choice of reactants. Another hypothesis can be the state of surface of the pristine material: maybe a fine layer of carbonate can react with $AlF_3$ to create a special layer.

Several publications report that the diffusion of transition metal initially deposited at the cathode material surface may be triggered by a heat treatment at high temperature. As an example, He et al. reported the diffusion of cobalt after a heat treatment of $Co(OH)_2$-coated $Mn_2O_3$ and $Li_2CO_3$ at a temperature of 750°C [56-57]. This leads to a spinel material $LiMnO_4$ with a cobalt doped surface. Other examples of surface doped active materials are reported in the literature especially with the titanium cation. In all case, this doping improves both electrochemical performances and cycle life. Lu et al. compared the electrochemical performances of a titanium coated and titanium surface doped $LiMn_2O_4$ cathode material and concluded that both treatments can limit the manganese dissolution [58]. In all cases, surface doped materials have an enhanced cycle life and a higher capacity than the pristine material. Okudur et al. produced several titanium surface materials by applying different temperatures on a $TiO_2$-coated $LiNi_{0.5}Mn_{1.5}O_4$ [59]. They highlighted that a low temperature of 500°C can be enough to make the titanium diffusion inside the surface structure of the lithium-rich layered oxide possible. The effects observed in these different publications are similar of ours, except for cycling life and

voltage fading. In all cases it seems that surface doped materials are promising and could be an alternative or a complement of classical coatings.

Manganese dissolution - migration - deposition process (DMD): The DMD mechanism is a well-documented phenomenon in the literature especially concerning manganese-enriched spinel cathode like $LiMn_2O_4$ or $LiNi_{0.5}Mn_{1.5}O_4$ oxides. However, several aspects of the fundamental mechanism of this phenomenon are still under debate especially concerning the oxidation state of Mn during the deposition step. When some authors report that metallic manganese is recovered on the anode side, others report that it is at the 2+ state. The link between capacity fade and the SEI modification is still under debate. Here, we report our observation based on lithium-rich layered oxide and silicon-graphite anode cells. Based on our characterisations, we assume that manganese and a very small amount of nickel are dissolved in the electrolyte during first cycles and migrate to the anode. The dissolution of manganese in the electrolyte is generally attributed to $Mn^{3+}$ in the material, which can disproportionate in $Mn^{4+}$ and $Mn^{2+}$. Then $Mn^{2+}$ can be dissolved in electrolyte. It is commonly admitted that the dissolved manganese corresponds to a loss of active material in the $LiMn_2O_4$ material because capacity is due to the $Mn^{3+}/Mn^{4+}$ redox. However this loss in active species in the cathode accounts for only 20-33 % of the overall capacity loss of spinel based cells [60]. The largest part of the total capacity loss is due to the modification of the SEI due to the manganese deposition. If all authors agree that the SEI modification induced by manganese contributes to increase the cell resistance, two main mechanisms are still under discussion: SEI growth due to metallic Mn or ion exchange between $Li^+$ and $Mn^{2+}$ in the SEI [39]. Even if the mechanism seems similar with lithium rich layered oxides and silicon graphite anode, we observe some little differences. In our case, XPS reveals that dissolved TM do not deposit on the anode all along the cycling. Mn and Ni could be detected in the SEI only after 10 cycles and not any longer after 20 cycles. Our hypothesis is that TM are dissolved only during the first cycles and then they catalyse side reactions and a new SEI is formed on the first one and hide the SEI with Mn(0) and Ni(0). Considering the presence of Ni and Li in our formula, which promotes a 4+ oxidation state to Mn, it can be argued

that the $Mn^{3+}$ content in the material may be too low to make the dissolution of TM during all cycling possible.

## 5. Conclusion

In lithium-ion pouch cells composed of $Li_{1.2}Ni_{0.2}Mn_{0.6}O_2$ and silicon graphite respectively for the cathode and anode, manganese and a very low amount of nickel are dissolved in the electrolyte and are deposited on the anode side only during the first cycles. After 10 cycles we observe that manganese is deposited on the anode side under its metallic form. Then, even if TM deposition stops after several cycles (because the few amount of $Mn^{3+}$ in the material formula), the TM deposited at the anode side degrades the electrolyte following new reactions. The product of this reaction is the creation of a thick carbonate based layer that completely covers the first SEI. At this step, it becomes difficult to detect the manganese at the anode surface. In the end, the resulting SEI completely insulates the anode and leads to an increase of cell resistivity. We assume that this phenomenon is the cause of the "sudden death effect" of our system. To solve this issue we tried to protect the $Li_{1.2}Ni_{0.2}Mn_{0.6}O_2$ particles by an $AlF_3$ coating, following a classical synthesis procedure described in the literature. Our synthesis results in a surface doped material (with Al and F), which appears to be inefficient to block the TM dissolution. We are now working to compare the influence between a real coating and a surface doped material to solve the manganese dissolution issue. For a more general conclusion, more publications in this field with finely characterized particles surfaces are needed. First, to conclude about the electrochemical enhancement due to surface treatment but also to highlight why similar treatment can result in a coating layer or in a doped surface.

## Acknowledgments

The study has been performed within the BEGREEN project. The authors gratefully acknowledge support from Pellenc Energy.

## References

[1] Christophe Pillot, The Rechargeable Battery Market: Value Chain and Main Trends 2020-2030, International Battery Seminar and Exhibit, March 11th 2021. https://www.internationalbatteryseminar.com/21/tutorials#3

[2] M.M. Thackeray, C.S. Johnson, J.T. Vaughey, N. Li, S.A. Hackney, Advances in manganese-oxide 'composite' electrodes for lithium-ion batteries, J. Mater. Chem. 15 (2005) 2257–2267. doi:10.1039/B417616M.

[3] A. Boulineau, L. Simonin, J.-F. Colin, E. Canévet, L. Daniel, S. Patoux, Evolutions of $Li_{1.2}Mn_{0.61}Ni_{0.18}Mg_{0.01}O_2$ during the Initial Charge/Discharge Cycle Studied by Advanced Electron Microscopy, Chem. Mater. 24 (2012) 3558–3566. doi:10.1021/cm301140g.

[4] C.S. Johnson, N. Li, C. Lefief, J.T. Vaughey, M.M. Thackeray, Synthesis, Characterization and Electrochemistry of Lithium Battery Electrodes: $xLi_2MnO_3 \cdot (1-x)LiMn_{0.333}Ni_{0.333}Co_{0.333}O_2$ ($0 \leq x \leq 0.7$), Chem. Mater. 20 (2008) 6095–6106. doi:10.1021/cm801245r.

[5] M. Rossouw, M. Thackeray, Lithium manganese oxides from $Li_2MnO_3$ for rechargeable lithium battery applications, Mater. Res. Bull. 26 (1991) 463–473. doi:10.1016/0025-5408(91)90186-P.

[6] Zhonghua Lu, and Zhaohui Chen, J.R. Dahn*, Lack of Cation Clustering in $Li[NixLi_{1/3-2x/3}Mn_{2/3-x/3}]O_2$ ($0 < x \leq 1/2$) and $Li[CrxLi_{(1-x)/3}Mn_{(2-2x)/3}]O2$ ($0 < x < 1$), (2003). doi:10.1021/cm030194s.

[7] J. Li, R. Shunmugasundaram, R. Doig, J.R. Dahn, In Situ X-ray Diffraction Study of Layered Li–Ni–Mn–Co Oxides: Effect of Particle Size and Structural Stability of Core–Shell Materials, Chem. Mater. 28 (2016) 162–171. doi:10.1021/acs.chemmater.5b03500.

[8] H. Koga, L. Croguennec, M. Ménétrier, K. Douhil, S. Belin, L. Bourgeois, E. Suard, F. Weill, C. Delmas, Reversible Oxygen Participation to the Redox Processes Revealed for $Li_{1.20}Mn_{0.54}Co_{0.13}Ni_{0.13}O_2$, J. Electrochem. Soc. 160 (2013) A786–A792. doi:10.1149/2.038306jes.

[9] H. Koga, L. Croguennec, M. Ménétrier, P. Mannessiez, F. Weill, C. Delmas, Different oxygen redox participation for bulk and surface: A possible global explanation for the cycling mechanism of $Li_{1.20}Mn_{0.54}Co_{0.13}Ni_{0.13}O_2$, J. Power Sources. 236 (2013) 250–258. doi:10.1016/j.jpowsour.2013.02.075.

[10] S. Muhammad, H. Kim, Y. Kim, D. Kim, J.H. Song, J. Yoon, J.-H. Park, S.-J. Ahn, S.-H. Kang, M.M. Thackeray, W.-S. Yoon, Evidence of reversible oxygen participation in anomalously high capacity Li- and Mn-rich cathodes for Li-ion batteries, Nano Energy. 21 (2016) 172–184. doi:10.1016/j.nanoen.2015.12.027.

[11] M. Sathiya, K. Ramesha, G. Rousse, D. Foix, D. Gonbeau, A.S. Prakash, M.L. Doublet, K. Hemalatha, J.-M. Tarascon, High Performance $Li_2Ru_{1-y}Mn_yO_3$ ($0.2 \leq y \leq 0.8$) Cathode Materials for Rechargeable Lithium-Ion Batteries: Their Understanding, Chem. Mater. 25 (2013) 1121–1131. doi:10.1021/cm400193m.

[12] M. Sathiya, G. Rousse, K. Ramesha, C.P. Laisa, H. Vezin, M.T. Sougrati, M.-L. Doublet, D. Foix, D. Gonbeau, W. Walker, A.S. Prakash, M. Ben Hassine, L. Dupont, J.-M. Tarascon, Reversible anionic redox chemistry in high-capacity layered-oxide electrodes, Nat. Mater. 12 (2013) 827–835. doi:10.1038/nmat3699.

[13] J.R. Croy, D. Kim, M. Balasubramanian, K. Gallagher, S.-H. Kang, M.M. Thackeray, Countering the Voltage Decay in High Capacity $xLi_2MnO_3 \bullet (1-x)LiMO_2$ Electrodes (M=Mn, Ni, Co) for Li+-Ion Batteries, J. Electrochem. Soc. 159 (2012) A781–A790. doi:10.1149/2.080206jes.

[14] J.R. Croy, S.-H. Kang, M. Balasubramanian, M.M. Thackeray, $Li_2MnO_3$-based composite cathodes for lithium batteries: A novel synthesis approach and new structures, Electrochem. Commun. 13 (2011) 1063–1066. doi:10.1016/j.elecom.2011.06.037.

[15] D. Peralta, J.-F. Colin, A. Boulineau, L. Simonin, F. Fabre, J. Bouvet, P. Feydi, M. Chakir, M. Chapuis, S. Patoux, Role of the composition of lithium-rich layered oxide materials on the voltage decay, J. Power Sources. 280 (2015) 687–694. doi:10.1016/j.jpowsour.2015.01.146.

[16] W. Zou, F.-J. Xia, J.-P. Song, L. Wu, L.-D. Chen, H. Chen, Y. Liu, W.-D. Dong, S.-J. Wu, Z.-Y. Hu, J. Liu, H.-E. Wang, L.-H. Chen, Y. Li, D.-L. Peng, B.-L. Su, Probing and suppressing voltage fade of Li-rich $Li_{1.2}Ni_{0.13}Co_{0.13}Mn_{0.54}O_2$ cathode material for lithium-ion battery, Electrochimica Acta 318 (2019) 875-882. doi.org/10.1016/j.electacta.2019.06.119

[17] Mengchu Yang, Bei Hu, Fushan Geng, Chao Li, Xiaobing Lou, Bingwen Hu, Mitigating voltage decay in high-capacity $Li_{1.2}Ni_{0.2}Mn_{0.6}O_2$ cathode material by surface K+ doping, Electrochimica Acta 291 (2018) 278-286. doi.org/10.1016/j.electacta.2018.09.134.

[18] W. Zhang, Y. Liu, J. Wu, H. Shao, Y. Yang, Surface Modification of $Li_{1.2}Mn_{0.54}Ni_{0.13}Co_{0.13}O_2$ Cathode Material with $Al_2O_3/SiO_2$ Composite for Lithium-Ion Batteries, J. Electrochem. Soc. 166 (2019) A863–A872. doi:10.1149/2.0171906jes.

[19] G. Zou, X. Yang, X. Wang, L. Ge, H. Shu, Y. Bai, C. Wu, H. Guo, L. Hu, X. Yi, B. Ju, H. Hu, D. Wang, R. Yu, Improvement of electrochemical performance for Li-rich spherical $Li_{1.3}[Ni_{0.35}Mn_{0.65}]O_2$+xmodified by $Al_2O_3$, J. Solid State Electrochem. 18 (2014) 1789–1797. doi:10.1007/s10008-014-2411-5.

[20] H. Meng, L. Li, J. Liu, X. Han, W. Zhang, X. Liu, Q. Xu, Surface modification of Li-rich layered $Li[Li_{0.17}Ni_{0.17}Co_{0.10}Mn_{0.56}]O_2$ oxide with $LiV_3O_8$ as a cathode material for Li-ion batteries, J. Alloys Compd. 690 (2017) 256–266. doi:10.1016/j.jallcom.2016.08.089.

[21] J. Meng, Q. Ma, L. Xu, Z. Wang, H. Xu, S. Zhang, Improving cycling stability and suppressing voltage fade of layered lithium-rich cathode materials via $SiO_2$ shell coating, Ionics. 25 (2019) 1979–1990. doi:10.1007/s11581-018-2673-5.

[22] D. Chen, F. Zheng, L. Li, M. Chen, X. Zhong, W. Li, L. Lu, Effect of $Li_3PO_4$ coating of layered lithium-rich oxide on electrochemical performance, J. Power Sources. 341 (2017) 147–155. doi:10.1016/j.jpowsour.2016.11.020.

[23] X. Zhang, X. Xie, R. Yu, J. Zhou, Y. Huang, S. Cao, Y. Wang, K. Tang, C. Wu, X. Wang, Improvement of the Cycling Stability of Li-Rich Layered Mn-Based Oxide Cathodes Modified by Nanoscale $LaPO_4$ Coating, ACS Appl. Energy Mater. 2 (2019) 3532–3541. doi:10.1021/acsaem.9b00287.

[24] T. Zhao, L. Li, R. Chen, H. Wu, X. Zhang, S. Chen, M. Xie, F. Wu, J. Lu, K. Amine, Design of surface protective layer of $LiF/FeF_3$ nanoparticles in Li-rich cathode for high-capacity Li-ion batteries, Nano Energy. 15 (2015) 164–176. doi:10.1016/j.nanoen.2015.04.013.

[25] S.-T. Myung, K. Izumi, S. Komaba, H. Yashiro, H.J. Bang, Y.-K. Sun, N. Kumagai, Functionality of Oxide Coating for $Li[Li_{0.05}Ni_{0.4}Co_{0.15}Mn_{0.4}]O_2$ as Positive Electrode Materials for Lithium-Ion Secondary Batteries, J. Phys. Chem. C. 111 (2007) 4061–4067. doi:10.1021/jp0674367.

[26] J.M. Zheng, J. Li, Z.R. Zhang, X.J. Guo, Y. Yang, The effects of $TiO_2$ coating on the electrochemical performance of $Li[Li_{0.2}Mn_{0.54}Ni_{0.13}Co_{0.13}]O_2$ cathode material for lithium-ion battery, Solid State Ion. 179 (2008) 1794–1799. doi:10.1016/j.ssi.2008.01.091.

[27] Y. Wu, A. Manthiram, High Capacity, Surface-Modified Layered $Li[Li_{(1-x)/3}Mn_{(2-x)/3}Ni_{x/3}Co_{x/3}]O_2$ Cathodes with Low Irreversible Capacity Loss, Electrochem. Solid-State Lett. 9 (2006) A221–A224. doi:10.1149/1.2180528.

[28] S.J. Shi, J.P. Tu, Y.Y. Tang, X.Y. Liu, Y.Q. Zhang, X.L. Wang, C.D. Gu, Enhanced cycling stability of $Li[Li_{0.2}Mn_{0.54}Ni_{0.13}Co_{0.13}]O_2$ by surface modification of MgO with melting impregnation method, Electrochimica Acta. 88 (2013) 671–679. doi:10.1016/j.electacta.2012.10.111.

[29] Y. Zhao, C. Zhao, H. Feng, Z. Sun, D. Xia, Enhanced Electrochemical Performance of $Li[Li_{0.2}Ni_{0.2}Mn_{0.6}]O_2$ Modified by Manganese Oxide Coating for Lithium-Ion Batteries, Electrochem. Solid-State Lett. 14 (2011) A1–A5. doi:10.1149/1.3496402.

[30] X. Guan, B. Ding, X. Liu, J. Zhu, C. Mi, X. Zhang, Enhancing the electrochemical performance of $Li_{1.2}Ni_{0.2}Mn_{0.6}O_2$ by surface modification with nickel–manganese composite oxide, J. Solid State Electrochem. 17 (2013) 2087–2093. doi:10.1007/s10008-013-2070-y.

[31] Y.-K. Sun, M.-J. Lee, C.S. Yoon, J. Hassoun, K. Amine, B. Scrosati, The Role of AlF3 Coatings in Improving Electrochemical Cycling of Li-Enriched Nickel-Manganese Oxide Electrodes for Li-Ion Batteries, Adv. Mater. 24 (2012) 1192–1196. doi:10.1002/adma.201104106.

[32] D. Chen, W. Tu, M. Chen, P. Hong, X. Zhong, Y. Zhu, Q. Yu, W. Li, Synthesis and performances of Li-Rich@$AlF_3$@Graphene as cathode of lithium ion battery | Electrochimica Acta, 193 (2016) 45-53. doi:10.1016/j.electacta.2016.02.043.

[33] S. Sun, Y. Yin, N. Wan, Q. Wu, X. Zhang, D. Pan, Y. Bai, X. Lu, $AlF_3$ Surface-Coated $Li[Li_{0.2}Ni_{0.17}Co_{0.07}Mn_{0.56}]O_2$ Nanoparticles with Superior Electrochemical Performance for Lithium-Ion Batteries, ChemSusChem. 8 (2015) 2544–2550. doi:10.1002/cssc.201500143.

[34] J.-H. Kim, M.-S. Park, J.-H. Song, D.-J. Byun, Y.-J. Kim, J.-S. Kim, Effect of aluminum fluoride coating on the electrochemical and thermal properties of $0.5Li_2MnO_3 \cdot 0.5LiNi_{0.5}Co_{0.2}Mn_{0.3}O_2$ composite material, J. Alloys Compd. 517 (2012) 20–25. doi:10.1016/j.jallcom.2011.11.117.

[35] X. Qu, Z. Yu, D. Ruan, A. Dou, M. Su, Y. Zhou, Y. Liu, D. Chu, Enhanced Electrochemical Performance of Ni-Rich Cathode Materials with $Li_{1.3}Al_{0.3}Ti_{1.7}(PO_4)_3$ Coating, ACS Sustainable Chem. Eng. 8 (2020) 5819−5830. doi:10.1021/acssuschemeng.9b05539.

[36] W.-W. Li, X.-J. Zhang, J.-J. Si, J. Yang, X.-Y. Sun, $TiO_2$-coated $LiNi_{0.9}Co_{0.08}Al_{0.02}O_2$ cathode materials with enhanced cycle performance for Li-ion batteries, Rare Met. 40 (2021) 1719–1726. doi:10.1007/s12598-020-01483-5.

[37] J. Zheng, M. Gu, J. Xiao, B.J. Polzin, P. Yan, X. Chen, C. Wang, J.-G. Zhang, Functioning Mechanism of $AlF_3$ Coating on the Li- and Mn-Rich Cathode Materials, Chem. Mater. 26 (2014) 6320–6327. doi:10.1021/cm502071h.

[38] S.-H. Yu, T. Yoon, J. Mun, S. Park, Y.-S. Kang, J.-H. Park, S.M. Oh, Y.-E. Sung, Continuous activation of $Li_2MnO_3$ component upon cycling in $Li_{1.167}Ni_{0.233}Co_{0.100}Mn_{0.467}Mo_{0.033}O_2$ cathode material for lithium ion batteries, J. Mater. Chem. A. 1 (2013) 2833–2839. doi:10.1039/C2TA00309K.

[39] C. Zhan, T. Wu, J. Lu, K. Amine, Dissolution, migration, and deposition of transition metal ions in Li-ion batteries exemplified by Mn-based cathodes – a critical review, Energy Environ. Sci. 11 (2018) 243–257. doi:10.1039/C7EE03122J.

[40] R. Cabanel, G. Barral, J. -P. Diard, B. Le Gorrec, C. Montella, Determination of the diffusion coefficient of an inserted species by impedance spectroscopy: application to the $H/H_x Nb_2O_5$ system, J Appl Electrochem 23 (1993) 93–97. doi:10.1007/BF00246943.

[41] V. Sharova, A. Moretti, T. Diemant ,A. Varzi, R. J. Behm, S. Passerini, Comparative study of imide-based Li salts as electrolyte additives for Li-ion batteries, Journal of Power Sources 375 (2018) 43-52. doi:10.1016/j.jpowsour.2017.11.045.

[42] E. Radvanyi, E. De Vito, W. Porcher, S. Jouanneau Si Larbi, An XPS/AES comparative study of the surface behaviour of nano-silicon anodes for Li-ion batteries, J. Anal. At. Spectrom. 29 (2014) 1120-1131. doi:10.1039/C3JA50362C

[43] C. Charton, J. Santos-Peña, A. Biller, E. De Vito, H. Galiano, M. Le Digabel, D. Lemordant, Reactivity of Succinic Anhydride at Lithium and Graphite Electrodes, J. Electrochem. Soc. 164 (2017) A1454-A1463. doi:10.1149/2.0621707jes.

[44] R. Tatara, P. Karayaylali, Y. Yu, Y. Zhang, L. Giordano, F. Maglia, R. Jung, J. P. Schmidt, I. Lund, Y. Shao-Horn, The Effect of Electrode-Electrolyte Interface on the Electrochemical Impedance Spectra for Positive Electrode in Li-Ion Battery, J. Electrochem. Soc. 166 (2019) A5090-A5098. doi:10.1149/2.0121903jes.

[45] M. C. Biesinger, B. P. Payne, A. P.. Grosvenor, L. W. M. Lau, A. R.Gerson, R. St.C.Smart, Resolving surface chemical states in XPS analysis of first row transition metals, oxides and hydroxides: Cr, Mn, Fe, Co and Ni, Applied Surface Science 257 (2011) 2717–2730. doi:10.1016/j.apsusc.2010.10.051

[46] S.Oswald, Binding energy referencing for XPS in alkali metal-based battery materials research (I): Basic model investigations, Applied Surface Science 351 (2015) 492–503. doi:10.1016/j.apsusc.2015.05.029.

[47] J. C. Jones, S. Rajendran, A. Pilli, V. Lee, N. Chugh, L. M. R. Arava, J. A. Kelber, In situ x-ray photoelectron spectroscopy study of lithium carbonate removal from garnet-type solid-state electrolyte using ultra high vacuum techniques, J. Vac. Sci. Technol. A 38 (2020) 023201. doi:10.1116/1.5128102

[48] T. Numata, C. Amemiya, T. Kumeuchi, M. Shirakata, M. Yonezawa, Advantages of blending $LiNi_{0.8}Co_{0.2}O_2$ into $Li_{1+x}Mn_{2-x}O_4$ cathodes, J. Power Sources. 97–98 (2001) 358–360. https://doi.org/10.1016/S0378-7753(01)00753-4.

[49] M. Xu, L. Zhou, Y. Dong, Y. Chen, A. Garsuch, B.L. Lucht, Improving the Performance of Graphite/ $LiNi_{0.5}Mn_{1.5}O_4$ Cells at High Voltage and Elevated Temperature with Added Lithium Bis(oxalato) Borate (LiBOB), J. Electrochem. Soc. 160 (2013) A2005. https://doi.org/10.1149/2.053311jes.

[50] S. Yamamoto, H. Noguchi, W. Zhao, Improvement of cycling performance in Ti substituted $0.5Li_2MnO_3$–$0.5LiNi_{0.5}Mn_{0.5}O_2$ through suppressing metal dissolution, J. Power Sources. 278 (2015) 76–86. https://doi.org/10.1016/j.jpowsour.2014.12.038.

[51] X. Jiang, Z. Wang, D. Rooney, X. Zhang, J. Feng, J. Qiao, W. Sun, K. Sun, A design strategy of large grain lithium-rich layered oxides for lithium-ion batteries cathode, Electrochimica Acta. 160 (2015) 131–138. https://doi.org/10.1016/j.electacta.2015.02.061.

[52] S. Komaba, N. Kumagai, Y. Kataoka, Influence of manganese(II), cobalt(II), and nickel(II) additives in electrolyte on performance of graphite anode for lithium-ion batteries, Electrochimica Acta. 47 (2002) 1229–1239. doi/10.1016/S0013-4686(01)00847-7.

[53] J.M. Zheng, Z.R. Zhang, X.B. Wu, Z.X. Dong, Z. Zhu, Y. Yang, The Effects of AlF3 Coating on the Performance of $Li[Li_{0.2}Mn_{0.54}Ni_{0.13}Co_{0.13}]O_2$ Positive Electrode Material for Lithium-Ion Battery, J. Electrochem. Soc. 155 (2008) A775–A782. doi:10.1149/1.2966694.

[54] K.J. Rosina, M. Jiang, D. Zeng, E. Salager, A.S. Best, C.P. Grey, Structure of aluminum fluoride coated $Li[Li_{1/9}Ni_{1/3}Mn_{5/9}]O_2$ cathodes for secondary lithium-ion batteries, J. Mater. Chem. 22 (2012) 20602–20610. doi:10.1039/C2JM34114J.

[55] H. Liu, D. Qian, M.G. Verde, M. Zhang, L. Baggetto, K. An, Y. Chen, K.J. Carroll, D. Lau, M. Chi, G.M. Veith, Y.S. Meng, Understanding the Role of $NH_4F$ and $Al_2O_3$ Surface Co-modification on Lithium-Excess Layered Oxide $Li_{1.2}Ni_{0.2}Mn_{0.6}O_2$, ACS Appl. Mater. Interfaces. 7 (2015) 19189–19200. doi:10.1021/acsami.5b04932.

[56] X.M. He, J.J. Li, Y. Cai, Y. Wang, J. Ying, C. Jiang, C. Wan, Preparation of spherical spinel $LiMn_2O_4$ cathode material for lithium ion batteries, J. Solid State Electrochem. 9 (2005) 438–444. doi:10.1007/s10008-004-0593-y.

[57] X. He, J. Li, Y. Cai, Y. Wang, J. Ying, C. Jiang, C. Wan, Preparation of co-doped spherical spinel $LiMn_2O_4$ cathode materials for Li-ion batteries, J. Power Sources. 150 (2005) 216–222. doi:10.1016/j.jpowsour.2005.02.029.

[58] J. Lu, C. Zhan, T. Wu, J. Wen, Y. Lei, A.J. Kropf, H. Wu, D.J. Miller, J.W. Elam, Y.-K. Sun, X. Qiu, K. Amine, Effectively suppressing dissolution of manganese from spinel lithium manganate via a nanoscale surface-doping approach, Nat. Commun. 5 (2014) 5693. doi:10.1038/ncomms6693.

[59] F.U. Okudur, J. D'Haen, T. Vranken, D.D. Sloovere, M. Verheijen, O.M. Karakulina, A.M. Abakumov, J. Hadermann, M.K.V. Bael, A. Hardy, Ti surface doping of $LiNi_{0.5}Mn_{1.5}O_{4-\delta}$ positive electrodes for lithium ion batteries, RSC Adv. 8 (2018) 7287–7300. doi:10.1039/C7RA12932G.

[60] C. Zhan, J. Lu, A. Jeremy Kropf, T. Wu, A.N. Jansen, Y.-K. Sun, X. Qiu, K. Amine, Mn(II) deposition on anodes and its effects on capacity fade in spinel lithium manganate–carbon systems, Nat. Commun. 4 (2013) 2437. doi:10.1038/ncomms3437.